HHS Public Access

Author manuscript

J Photochem Photobiol B. Author manuscript; available in PMC 2018 August 01.

Published in final edited form as:

J Photochem Photobiol B. 2017 August ; 173: 282–290. doi:10.1016/j.jphotobiol.2017.06.001.

Spectral Selectivity Model for Light Transmission by the Intermediate Filaments in Müller Cells

Igor Khmelinskii[1], **Tatiana Golubeva**[2], **Elena Korneeva**[3], **Mikhail Inyushin**[4], **Lidia Zueva**[5,6], and **Vladimir Makarov**[6]

[1]Universidade do Algarve, FCT, DQF and CIQA, 8005-139, Faro, Portugal

[2]Lomonosov Moscow State University, Department of Vertebrate Zoology, Moscow 119992, Russia

[3]Institute of Higher Nervous Activity and Neurophysiology, Russian Academy of Sciences, Butlerova st., 5a, 117485, Moscow, Russia

[4]Universidad Central del Caribe, Bayamón, Puerto Rico

[5]Sechenov Institute of Evolutionary Physiology and Biochemistry, Russian Academy of Sciences, St. Petersburg, Russia

[6]University of Puerto Rico, Rio Piedras Campus, PO Box 23343, San Juan, PR 00931-3343, USA

Abstract

Presently we continue our studies of the quantum mechanism of light energy transmission in the form of excitons by axisymmetric nanostructures with electrically conductive walls. Using our theoretical model, we analyzed the light energy transmission by biopolymers forming optical channels within retinal Müller cells. There are specialized intermediate filaments (IF) 10 – 18 nm in diameter, built of electrically conductive polypeptides. Presently, we analyzed the spectral selectivity of these nanostructures. We found that their transmission spectrum depends on their diameter and wall thickness. We also considered the classical approach, comparing the results with those predicted by the quantum mechanism. We performed experimental measurements on model quantum waveguides, made of rectangular nanometer-thick chromium (Cr) tracks. The optical spectrum of such waveguides varied with their thickness. We compared the experimental absorption/transmission spectra with those predicted by our model, with good agreement between the two. We report that the observed spectra may be explained by the same mechanisms as operating in metal nanolayers. Both the models and the experiment show that Cr nanotracks have high light transmission efficiency in a narrow spectral range, with the spectral maximum dependent on the layer thickness. Therefore, a set of intermediate filaments with different geometries may provide light transmission over the entire visible spectrum with a very high (~90%) efficiency. Thus, we believe that high contrast and visual resolution in daylight are provided by the quantum mechanism of energy transfer in the form of excitons, whereas the

Corresponding author: Dr. Vladimir I. Makarov, Phone: (1)787-529-2010, vmvimakarov@gmail.com.

ultimate retinal sensitivity of the night vision is provided by the classical mechanism of photons transmitted by the Müller cell light-guides.

Graphical abstract

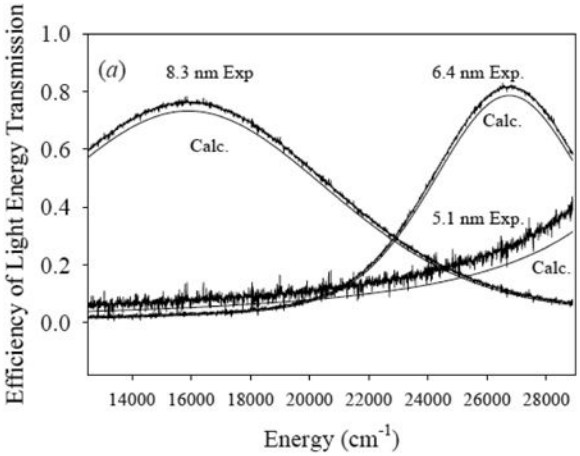

I. Introduction

Vertebrates have an inverted retina, with the photo-sensitive layer of photoreceptor cells located on its far side. Thus, light has to pass through the entire retina before interacting with rhodopsin molecules in the membranes of the outer segments of the photoreceptor cells, usually of several spectral types. Thus, the main issue, extensively discussed for over 100 years, deals with an explanation for the high contrast and resolution achieved in eyes with an inverted retina. Namely, light has to traverse up to several hundreds of micrometers through the retina, without scattering or absorption on the organelles of different cells packed into this space. The retinal thickness was measured in close-to-*in vivo* conditions by optical coherent tomography (OCT) [1]. Tao Li et al. (2016) found that the average retinal thickness in guinea pig is in the range of 170 – 250 μm. Buttery et al. [2] reported in 1991 the same value being in the range of 124-157 μm, with the average of ca. 142 μm. This value slightly exceeds that obtained for histological preparations (105-151 μm, with ca. 134 μm average) [3,4]. Franze et al. (2007) reported that freshly dissected guinea pig eyes have retinal thickness of ca. 150 μm [5]. The differences between the results reported by various authors may be attributed to different methods and/or retinal zones used in the measurements.

The data obtained by histological methods show that vascular retinas in mammals are usually thicker (220-250 μm) than avascular retinas (140-170 μm) [3,4]. The retina is thicker in birds as compared to mammals. Indeed, the retinal thickness of 300-400 μm was measured in two species of hawks [6]. Retinal thickness may be estimated from the length of the Müller cells, with the results depending on the cell location within the retina and typically lower than the *in vivo* values due to the fixation treatment. The Müller cell length as estimated by the analysis of retinal images is 163 μm in cat and dog, 143 μm in human, and 110 μm in rat (vascular retinas), and 79 μm in echidna and 113 μm in rabbit (avascular

retinas) [7], where the retinal Müller cells were labeled by eight monoclonal antibodies. Thus, we need a better understanding of light transport within the retina, which we shall provide by implementing some of our previously proposed concepts and approaches.

Govardovskii et al. (1981) [8] studied retinal light transmission using a model based on classical electrodynamics. The effect of the refractive structures of the photoreceptor inner segment on the directional sensitivity was studied using microwave model systems. It was shown that the main role of the cell organoids is to narrow the directional sensitivity curve, reducing the effects of light scattering and increasing the depth of focus.

A detailed analysis of the retinal structure along with the analysis of the retinal light transmission mechanisms was presented in the book by Reichenbach and Bringmann [9]. Discussing the possible role of glial Müller cells in the retinal light transmission, they proposed that light transmission is mainly provided by the Müller cells, treated as classical light guides (optical fibers) by Franze et al. (2007) [10]. However, no structural or functional mechanism of light transmission by Müller cells has ever been proposed. The main issue that we have already addressed earlier [8-10] is the apparent contradiction between the ideas of classical electrodynamics and the retinal structure.

Detailed morphological studies of Müller cells in Pied flycatcher were reported by Zueva et al. (2016) [11]. Using an electron microscope, authors traced special intermediate filaments through the entire length of Müller cells [11]. Therefore, we suggested that these intermediate filaments, spanning the entire cell from the endfoot adjacent to the vitreous body to the apical process end that interacts with retinal cones, directly participate in the transmission of luminous energy [12]. Taking into account the IF diameter of 10-18 nm, while the wavelength of the near UV - VIS light is in the 800 – 360 nm range, the individual IFs are unable to transmit light by the classical mechanism. Therefore, we previously proposed a quantum mechanism of the light energy transport by the IFs of the Müller cells, in the form of excitons [12]. We also proposed theoretically and demonstrated experimentally in a model system [13] that properly structured intermediate filaments could work as polarization filters. All of these data in conjunction suggest that intermediate filaments (IFs) may be responsible for light transmission in a variety of cells in different species. Most of the modeling experiments and theoretical models never considered intermediate filaments as the retinal light-guides, while accounting for the cellular organoids in the photoreceptor optical properties. However, every one of the listed experimental studies notes the very high efficiency of retinal light transmission. To explain this result, we have earlier proposed the quantum model of light transmission by an inverted retina, which we further develop here [11-13].

Namely, we proposed a quantum mechanism (QM) for the electromagnetic field (EMF) energy transmission by a waveguide [12], in the form of a nano-capillary with conductive walls, with its diameter significantly smaller than the EMF wavelength. As we shall describe shortly, such structures indeed exist in live cells in the form of intermediate filaments. Thus, our approach is a detailed quantum representation of the plasmon-polaron theory. Earlier, we presented a review of published reports on this theory and its applications [12], which, therefore, we shall not describe in any detail here. We thus found that the QM can explain

the high efficiency of EMF energy transmission by IF waveguides, if we optimize the shape of the latter at both of its ends. We also noted that the QM explains the light transmission of the Müller cells (MC), without the exact knowledge of the waveguide structure [11]. We assumed that the optically conductive structures in the MCs are formed by electrically conductive intermediate filaments, built of polypeptides, thus our model represents each IF as an axisymmetric tube with electrically conductive walls. Note that spectral selectivity of the Müller cell optical channels is an interesting property that may enhance the spectral selectivity of the respective photoreceptor cells. Optical selectivity of different nanoscale systems has been explored quite intensively [14-25], with several models proposed [26,27]. However, none of the available reports has considered the mechanism recently proposed by Makarov et al. [12]. Therefore, presently we use our quantum model to explore the spectral selectivity in axisymmetric nanoscale systems [12]. The quantitative modeling results are compared to the quantitative data obtained using the classical model. Presently we report an experimental test of spectral selectivity using model optical waveguides made of nanometer-thick chromium tracks of rectangular cross-section. Quantum confinement (QC) effects are observed in nanoscale systems, as we have recently described in conductive nanolayers [26,27]. We found that excitations (excitons) propagate in such systems over macroscopic distances on the nanosecond time scale, with the entire sample surface emitting homogeneously after its localized excitation [26,27]. We reported similar effects in Cr tracks, with the effective transmission spectrum dependent on the metal nanolayer thickness.

Presently we explore the spectral selectivity and light transmission efficiency by intermediate filaments in theoretical models. We find that the entire visible spectrum may be transmitted by a mixture of appropriate intermediate filaments, with their superimposed spectra covering the required spectral range. We also report high efficiencies of the EMF energy transmission in such system, up to 80 – 90%. Thus, presently we theoretically analyze the spectral selectivity of the IFs in Müller cells, using the models and methods developed earlier [12], and explore such ideas experimentally, studying the transmission spectra of Cr metal nanotracks with different thickness. We conclude that metal nanotracks provide a useful model for testing the presently developed theoretic approach, as the model was able to reproduce the experimental spectra.

Note that the presently proposed quantum mechanism of the light energy transfer in an inverted retina is a mechanism additional to the conventional classical light-guide mechanism. We infer that the quantum mechanism is important for daytime vision, providing utmost contrast and resolution, whereas the classical mechanism works in night-time vision where the scattered light is not such a priority and the highest possible resolution can be traded for the ultimate low-light sensitivity. We therefore believe that the quantum mechanism is responsible for the high contrast and resolution in the daylight vision. Here we analyze the spectral selectivity of the individual IFs and their transmission efficiency.

II. Theoretical models and methods

a) General statements

We analyze spectral selectivity of the IFs in Müller cells using models and methods developed earlier [12]. Note that diameter and wall thickness of the IFs are much smaller

than the wavelength of visible light. Our model employs QC to describe the EMF energy transmission by the IFs in the form of excitons [12], used presently to analyze the spectral selectivity of the IFs in function of their diameter, wall thickness, and other geometrical parameters. We applied the previously developed approach to axisymmetric nanoscale systems, similar to those considered earlier [12]. The earlier developed theoretical model addressed an axisymmetric waveguide described by the $D_{\infty h}$ point group [12].

Cylindrical waveguide is a specific example of a system with $D_{\infty h}$ symmetry. We assumed a cylinder with the radius r_0 and an electrically conductive external layer with the thickness ρ. We found that the problem may be conveniently solved in separable variables using the cylindrical coordinates r, φ and z [12]. We further found [12] that quantum confinement is observed at sufficiently small ρ values, with the quantization of the electronic states within the cylindrical conductor significantly affecting the light transmission by the waveguide, and the electronic state structure dependent on both ρ and r_0. The projection Λ of the electronic orbital angular momentum on the symmetry axis is conserved. Thus, for $\Lambda = 0$ the energies of the discrete electronic states in the cylindrical waveguide are given by [12]:

$$k(r_0+\rho)=\mathrm{Arctg}\left[\left(1+\frac{\rho}{r_0}\right)tg(kr_0)\right]+n\pi \quad (1)$$

where n =1, 2, 3,…, is the quantum number,

$$k^2=\frac{2m_e^{\mathrm{eff}}}{\hbar^2}E_{r,\varphi} \quad (2)$$

here, k is the wave vector, m_e^{eff} is the effective electron mass and $E_{r,\varphi}$ is the state energy. The equation (1) may only be solved numerically. Addressing the more complex case of $\Lambda \neq 0$, the same energies are given by [12]:

$$E_{nk\Lambda}=\left\langle \psi_{nk\Lambda}(r,\varphi,z)\left|\hat{H}\right|\psi_{nk\Lambda}(r,\varphi,z)\right\rangle \quad (3)$$

where the wavefunction is given by:

$$\psi_{nk\Lambda}=C_0\sqrt{\frac{2}{L}}r^{\Lambda}\left(\frac{1}{r}\frac{d}{dr}\right)^{\Lambda}\left[\left(\frac{\mathrm{Sin}(kr)}{kr}-\frac{1}{kr_0}tg(kr_0)\mathrm{Cos}(kr)\right)\right]\times e^{i\Lambda\varphi}\mathrm{Sin}\left(\frac{\pi n}{L}z\right) \quad (4)$$

The position of the spectral maximum of the lowest electronic transition (Δn =1; $\Delta\Lambda$ = 0,±1) in function of r_0 and ρ was calculated using a home-made FORTRAN code.

b) Numerical analysis of a cylindrical waveguide

We calculated the spectral absorption maximum in function of r_0 for a cylindrical device 100 μm long (typical length of a MC), at different thickness values: ρ = 0.5, 1.0, 2.0 and 4.0 nm, with the results shown in Figure 1.

Figure 1 shows that the spectral absorption maximum shifts to lower energies with the increased device radius, the same happens with the increased wall thickness ρ. Note also that transitions with $\Delta\Lambda = 0$ have higher energy than those with $\Delta\Lambda = 1$. As we found earlier, the emission spectrum should coincide with the absorption spectrum, provided the excited-state relaxation is slow [12]. Also, the transitions $(n, \Lambda) \rightarrow (n+1, \Lambda)$ should have higher energy than the transitions for $(n, \Lambda) \rightarrow (n+1, \Lambda+1)$, the same initial state (n, Λ). Therefore, it should be possible to obtain spectral selectivity for any part of the UV/VIS/IR spectrum by varying the waveguide geometry. This conclusion follows from the analysis of a simple model for the cylindrical waveguide with an electrically conductive external nanolayer, shown in Figure 1.

Modeling of a waveguide with $D_{\infty h}$ symmetry of arbitrary shape—The same conclusion regarding tuning the spectral selectivity by geometry may be extended to waveguides of arbitrary shape, as we found using the earlier proposed models [12], with the results shown in Figure 2.

Here, r_0 is the internal radius of a hollow electrically conductive cylindrical section in the middle of the waveguide, ρ is its thickness, L_2 is its length, L_1 is the length of the entire waveguide, $L_3 = \frac{L_1 - L_2}{2}$ is the length of the expanding input and output sections, R is the curvature radius of the external surface of the waveguide input and output area. The r and z variables are not separable in this model, therefore, we can only solve the problem numerically. Here we considered the case $r_0 \gg \rho$.

The calculations were done for ρ = 0.5 and 1.0 nm; r_0 = 5 nm; L_1 = 100 μm; L_2 = 99.99 μm; L_3 = 5 nm; R = 5.5 nm. Figure 3 shows the calculated absorption efficiency, the energy transmission efficiency and the EMF emission efficiency spectra, with its caption listing the parameter values.

The calculated bands were fitted by a Gaussian function

$$I = Ae^{-\left(\frac{\omega-\omega_0}{\sigma}\right)^2}, \quad (5)$$

with the values of the fitting parameters presented in Table 1.

Figure 3 and Table 1 show that the spectra overlap quite strongly with the spectral transmission band appearing either in UV (3a) or VIS (3b) spectral range. Thus, we conclude that optical waveguides with conductive walls may function as efficient optical filters, with the transmission range dependent on the waveguide parameters. We should also consider the mechanism of the bandwidth formation, as our model disregards the formation

of the homogeneous transition line width. Detailed numerical analysis of our models demonstrated that the spectral profiles of the absorption, transmission and emission spectra depend on the boundary conditions, or else on the geometrical structure of our system. For instance, zero bandwidth is obtained for a thin-walled hollow cylinder, while for the structure of Fig. 2 and the parameter values of Table 1, we obtain a finite band width. In the latter case, the spectral profile includes several transitions, with their contributions distributed over the band profile. We also note in Figure 3 and Table 1 that the energy transmission and emission band maxima are slightly red-shifted as compared to the absorption band maximum. This may also be explained by the effect of the boundary conditions upon the calculated wavefunctions.

c) Optimized waveguide configuration

Until now, we were analyzing the cylindrical waveguide and the waveguide of Figure 2. Next, we shall consider the waveguide with a spherical cap in the output section (see Figure 4), as such structure better corresponds to the known structure of the Ifs [12]. This gives us the rationale to investigate the light transmission by the waveguide of Figure 4.

In Figure 4a, L_1 = 100 μm is the total length, L_2 = 99.995 μm is the length without the input section, r_0 = 5 nm, ρ = 0.5 nm, $R = r_0 + \rho$ nm is the external radius of the tube, the output section is a hemisphere with the external radius R, internal radius r_0 = 5 nm and wall thickness ρ, which is the variable parameter, the parameter R' is the curvature radius of the input section, also variable.

The properties of the structure in Figure 4 were analyzed using suitably adapted FORTRAN code developed earlier [12], to calculate the integrated wavelength dependence of the EMF transmission efficiency. We analyzed the efficiency dependence on R', performing numerical analysis for several parameter sets, all listed in the caption to Figure 5 that shows the results.

Compared to the previous simulations [12], the data of Figure 5 demonstrate a higher efficiency of the EMF transmission. Therefore, the device in Figure 4 apparently has a better design than that in Figure 2. Probably, the transmission efficiencies in Müller cells may exceed 90%, although the extremely high efficiencies should not be critical for the quantum mechanism of light energy transmission, as this mechanism is most important for the daytime vision. The data obtained demonstrate the very high light transmission efficiency by nanostructured waveguides, which we believe exist in Müller cells in the form of IFs.

We also calculated the absorption, transmission, and emission spectra for two different parameter sets: (a) ρ = 1.0 nm, r_0 = 5 nm, $R' = R$ = 6 nm, L_1 = 100 μm, L_2 = 99.995 μm and (*b*) ρ = 4.0 nm, r_0 = 5 nm, $R' = R$ = 9 nm, L_1 = 100 μm, L_2 = 99.995 μm. The resulting spectra are shown in Fig. 6.

The spectral bands presented in Figure 6 were fitted by a Gaussian function (5). The values of the fitting parameters ω_0 and σ are listed in Table 2.

We see from Figs. 6a, 6b and Table 2 that the maxima in the transmission and emission spectra are slightly shifted to the red as compared to the respective absorption band. As we

already noted, these results may be explained by the effects of the boundary conditions existing in the input and output sections of the waveguide. Figure 6 also shows high transmission efficiencies with smaller shifts in the spectral maximum, compared to the results of Figures 3a and 3b. Thus, we once again conclude that the structure of the device of Figure 4 is better optimized for the EMF energy transmission than that of Figure 2. Note that the width of the spectral transmission curve increases with ρ, the conductive nanolayer thickness (Figure 6b), accompanied by a reduced transmission efficiency. Probably, this latter case corresponds more closely to the reality, as the structure of a single IF fiber resembles that of a cylinder with a thick conductive wall [28,29]. In addition, the resulting wider spectral transmission curve is better adapted to the absorption spectra of the visual pigments that are quite wide [30]. However, as we will show below, using a superposition of the transmission spectra of a set of IFs with different narrow transmission spectra (Figure 6a), we may also obtain a wide transmission spectrum adequate for the requirements of the visual system, while retaining high overall light transmission efficiencies (up to 90 %).

As we already noted, classical electrodynamics cannot explain light transmission by waveguides with diameter much less than photon wavelength; instead, we are describing the energy transfer in the form of the excited states – excitons. To support this idea, we shall quantitatively compare the presently developed quantum mechanism with the classical light transmission mechanism, using the same waveguides, as presented in the following section.

d) Classic model of light transmission by optical fibers

Maxwell equations for the electromagnetic wave propagation in a homogeneous medium may be presented as follows:

$$\begin{gathered}\left(c^2\nabla^2-\frac{\partial^2}{\partial t^2}\right)\overrightarrow{E}=0\\ \left(c^2\nabla^2-\frac{\partial^2}{\partial t^2}\right)\overrightarrow{B}=0\\ c=\frac{1}{\sqrt{\mu_0\varepsilon_0}}\end{gathered} \qquad (6)$$

To investigate the efficiency of the EMF energy transmission by optical nanochannels, we analyzed a model of two coaxial optical fibers, with the constant diameter of the first d_1 =1260 nm and variable diameter d_2 of the second, with $d_2 < d_1$. The two fibers are optically aligned along the common axis and in direct end-to-end contact. The two fibers have equal values of $\varepsilon = \varepsilon_0$ and $\mu = \mu_0$. The input power of coherent radiation into the first fiber at λ= 630 nm was variable in the 5 – 10 μW range. The energy transmitted from the first to the second fiber was multiplied by the normalizing factor d_1^2/d_2^2 correcting for the aperture losses. To study the efficiency of the EMF energy transmission in this system, we numerically analyzed the equation for the electric field component:

$$\left(c^2\nabla^2-\frac{\partial^2}{\partial t^2}\right)\overrightarrow{E}=0 \qquad (7)$$

with the Laplace operator presented in the cylindrical coordinates as follows:

$$\Delta=\nabla^2=\frac{\partial^2}{\partial r^2}+\frac{1}{r}\frac{\partial}{\partial r}+\frac{1}{r^2}\frac{\partial^2}{\partial \varphi^2}+\frac{\partial^2}{\partial z^2} \quad (8)$$

defining the following boundary conditions at the interface of the two fibers:

$$\begin{gathered}\left|\overrightarrow{E}_{1,b}\right|^2=\left|\overrightarrow{E}_{2,b}\right|^2 \\ c=\frac{1}{\sqrt{\mu_0\varepsilon_0}} \\ W_{1,b}=\frac{\pi d_1^2}{4}\left|\overrightarrow{E}_{1,b}\right|^2 \\ W_{2,b}=\frac{\pi d_2^2}{4}\left|\overrightarrow{E}_{2,b}\right|^2\end{gathered} \quad (9)$$

The results of the numerical analysis of the EMF energy transmission by this system are shown in Figure 7.

We see that at higher d_1/d_2 the transmitted EMF power drops almost to zero at d_2 < 79 nm with the half-width of the plot independent on the input power. Since the diameter of the MC intermediate filaments is only 10-18 nm, we conclude that the classical model does not describe the light transmission by separate intermediate filaments. Better results are produced by the quantum mechanism of exciton transport [12], which we use in our theoretical analysis. Thus, classical electrodynamics has limitation by optical waveguide diameter, and can not be used to explain the light transmission by individual IFs in Müller cells.

Thus, our theoretical analysis demonstrates that waveguides with 10-18 nm diameter and electrically conductive walls may work as bandpass optical filters, with the band parameters depending on geometry. The following section demonstrates these ideas implemented in a model waveguide constructed of a metal nanotrack.

III. Experimental testing of the model

We already discussed our theoretical model for the spectral selectivity of optical waveguides. We shall use this model to predict the properties of the intermediate filaments, which apparently transmit light in various transparent cells, Müller cells included. Presently, we are unable to experiment on real biological systems or model nanostructured systems such as carbon nanotubes; therefore, we carried out the experimental measurements of the transmission spectra in model systems that use chromium (Cr) metal track with 0.1 × 1.0 cm^2 size and variable nanothickness. We deposited the Cr pattern on a circular AlN substrate, connecting two optical light guides to the two end zones of the Cr track created, perpendicular to its surface. The active diameter of the light guides was 0.5 mm. Thus, we recorded the transmission spectra of the Cr tracks using the presently described approach. These experiments do not exactly reproduce the structure and properties on the IFs, and

therefore can't be projected directly onto the respective biological systems. However, they can be used to test our theoretical model adapted to a rectangular waveguide profile, and were performed with this very objective in mind.

(a) Experimental methods and techniques

We used commercial AlN substrates 12.5 mm in diameter and 1.5 mm thick (Valley Design Corp.) to deposit the Cr tracks with 0.1 cm × 1.0 cm surface area and a pre-determined thickness in the nm range. We used a commercial Cr target (Sigma/Aldrich) to produce nanotracks on a commercial sputtering/thermo-evaporation Benchtop Turbo deposition system (Denton Vacuum). We used a Cu foil mask to deposit Cr tracks of certain dimensions, controlling the track thickness by XRD. We calibrated the XPert MRD system (PANalytic) by standard nanofilms of the same material. The estimated absolute uncertainty of the Cr track thickness measurement was 7%; the relative uncertainties were much smaller, determined by the shutter opening times of the deposition system.

We recorded the transmission spectra on a Hitachi U-3900H UV-Visible Spectrophotometer. The spectral peak maxima and widths were located using the PeakFit software (Sigmaplot). The AlN substrates with Cr tracks were reproducibly installed into a special holder manufactured of blackened Al. Two multi-mode light guides with the active diameter of 0.5 mm were installed into Al holders as shown in Figure 8a. Note that these light guides are optically transparent in the visible special range only (800 to 445 nm).

The light guides were optically connected to the ends of the Cr track. The other ends of the light guides were mounted into the lens module interfacing the sample to the spectrophotometer (see Figure 9a). The latter module was reproducibly installed into the optical cell area of the spectrophotometer. Thus, the transmission spectra were recorded using the optical scheme shown in Figure 9a. The background absorption used to correct the transmission spectra was recorded using the optical scheme of Figure 9b, with the two light guides connected directly to each other.

(b) Experimental results and analysis

Three samples of the Cr nanoassembly were tested, with the following dimensions of the Cr nanotracks: (*a*) 0.1 × 1.0 cm^2 × 5.1 nm, (*b*) 0.1 × 1.0 cm^2 × 6.4 nm, and (*c*) 0.1 × 1.0 cm^2 × 8.3 nm. The transmission spectra of these samples, recorded using the device schematically shown in Figure 8, are presented in Figure 9. The transmission spectrum of the sample (*a*) was multiplied by the factor of 50, to show the transmission growing in function of the photon energy. We see that the sample (*a*) does not transmit visible light. Apparently, what we see is the tail of the transmission band with its maximum located in the UV. The transmission band shifts into the visible for the thicker Cr tracks, as seen in Figure 9a. The respective band maxima were located using the Peak-Fit software for the spectra of the samples (*b*) and (*c*), at 26757 and 15895 cm^{-1} with the bandwidths of 3578 and 6705 cm^{-1}, respectively.

The theoretical model developed earlier for axisymmetric optical waveguides [12] and here was modified to describe a rectangular nanotape, using the same physical ideas, with the bandwidth determined by the interactions between the discrete quantum states and the quasi-

continuum dense spectrum. The earlier developed FORTRAN code [12] was suitably modified for the new waveguide geometry. Figure 9a shows the numerically calculated transmission spectrum. An acceptable agreement between the experimental and calculated plots was obtained for the effective electron mass of $0.047 m_e$ and for the $n' = 9 \leftarrow n'' = 8$ electronic transitions in the (*b*) and (*c*) samples. Using the estimated effective electron mass, we reproduced the transmission spectrum for the sample (*a*), where the $n' = 8 \leftarrow n'' = 7$ electronic transition produces the best fit to the recorded band tail. This yields the maximum and the bandwidth for the transmission peak at 37587 cm^{-1} and 1378 cm^{-1}, respectively (see Figure 9b).

These results demonstrate that the proposed model is in fact capable of properly describing the light transmission by nanosized structures, including such properties as spectral selectivity. We believe that the same mechanisms operate in the optical waveguides, existing in biological systems and composed of intermediate filaments. Note that the 1D quantum confinement, used to interpret the presently obtained experimental data, was studied in detail earlier [26,27]. Although the experiments reported do not deal with IFs in Müller cells, the same quantum confinement phenomena operate in both these systems, and we do observe the light energy transport by excitons in our model experiments, which should also operate in the IFs. To obtain a model with 2D quantum confinement, closer to what is happening in IFs, we plan to use carbon nanotubes (CNTs) with different number of nanolayers. Note that spectral and excitonic properties of CNTs should be very similar to those of the IFs, as 2D quantum confinement operates in both, and both being electrically conductive, CNTs due to their conjugated **π**-system, and IFs due to their protein content [12].

IV. Discussion

We investigated the spectral selectivity of the EMF transmission by the optical waveguides (intermediate filaments), with the waveguide diameter much smaller than the EMF wavelength. Presently we introduce a model based on quantum confinement in nanostructured conductive materials [12]. This QC model was used to explore the EMF energy transmission by cylindrical waveguides and more complex systems with axial symmetry (see Figures 2 and 4). In addition, we considered a classic electrodynamics model of the two connected light guides with different diameters. Using this model, the transmitted power was calculated in function of the diameter ratio of the two light guides. We concluded that classic electrodynamic model is unable to account for the light transmission over nanostructured IF waveguides.

Previously we noted [12] that the QC model is an extension of the quasiclassic plasmon-polaron theory [31-33]. Light transmission in nanowires, nanotubes and similar systems was partially analyzed using the plasmon-polaron theory [31,32], with the transmission spectrum dependent on the wire diameter. The transmission spectra of the nanowires are significantly wider [26,27,31] than those obtained here and previously [12] for the thin-walled tubes, while comparable to the spectra obtained for thick-walled tubes (see Figure 6b and 9a). Thus, the QC model produces the results that seem quite reasonable, and should work well for the systems shown in Figures 2 and 4.

The electric conductivity of proteins has been reported earlier [34]. The protein structure facilitates long-range electron transfer in solutions and in dry solid state, with the electric currents much higher than those recorded for saturated-bond compounds with comparable sample thickness. Indeed, electric conductivity of proteins is comparable to that of nanowires made of carbon nanotubes [35]. Therefore, our comparison of the optical properties of the IFs and CNT is as well supported by the conductivity results reported earlier [35]. The cylindrically symmetric structure of the intermediate filaments resembles that of nanotubes, with low-density core and high-density walls, according to the X-ray diffraction data [36]. The specific beaded intermediate filaments of the eye fiber cells have a more complex arrangement, with periodic changes in their external diameter from 10 to 12 nm; still, they retain the cylindrically symmetric core and other important features of the protein filaments [37]. Thus, the currently proposed QC model should be applicable to intermediate filaments, wire-like biological structures built of proteins and present in many types of cells. The experimental device tested in the present study demonstrated that the proposed quantum mechanism of light transmission by optical waveguides should operate in nano-sized intermediate filaments. It is very interesting to compare the optical properties of the special IFs discussed here to those of carbon nanotubes, whose optical properties were extensively studied [38-44]. Note that π-conjugated carbon systems are good electric conductors, typical examples being single-wall carbon nanotubes (SWCNTs) and graphene [44]. Since SWCNTs have axial symmetry with electrically conductive walls, they present a reasonable model for our waveguides and their spectral selectivity, which should depend mostly on their diameter and weaker on the chemical structure. SWCNT is a hollow tube made of a one-atomic-layer wrapped-around graphene sheet. The wrapping direction may be described by the chiral vector (***n, m***), denoting the number of unit vectors along two directions in the crystal lattice of the graphene sheet [37]. Thus, a tube with $n = m$ (chiral angle = 30°) is an armchair tube, etc. A tube with $m, n \gg 1$ and $|m - n| = 3k$ has metallic conductivity [38]. The diameter d of the SWCNT is given by

$$d = \frac{c}{\pi}\sqrt{(n+m)^2 - mn,} \quad (10)$$

where $c = 0.246$ nm [44]. The optical absorption spectrum of the SWCNTs includes several electronic transitions: $v_2 \rightarrow c_2$ (E_{22}) or $v_1 \rightarrow c_1$ (E_{11}), etc. [38-40]. The transitions are relatively sharp and may identify nanotube types. Interestingly, the plasmon line in the absorption spectrum of the SWCNT with $d = 12$ nm is at ca. 4.5 eV [38], in reasonable agreement with the quantum calculations for an electrically conductive tube of the same diameter (5.3 eV) [12]. Although it is obvious that diameter and conductive nanolayer thickness are the most important properties of the structure, we cannot expect the properties of the IFs in MC to exactly coincide with those of CNTs with different number of the single wall carbon nanolayers, as already noted. However, taking into account the axial symmetry of both the IFs and CNTs, along with the electric conductivity of their walls, they both may be expected to efficiently transmit light by the quantum mechanism, in the form of excitons. We shall study these phenomena in more detail in future.

Note that no information on the electric conductivity of the IFs is available at this time. Nevertheless, many polypeptides do exhibit very high electric conductivity [34], as also reported in a review [45]. Therefore, we presume that the specialized IFs are in fact electrically conductive, thus our theoretical models should provide a valid description of light transmission by the IFs [12,13].

The models we developed here and earlier [11,12] describe hollow axially symmetric structures. Note that the thickness of the IF conductive layer is described by the theoretic parameter ρ. Since the IF diameter is confined to the 10 – 18 nm range, the spectral selectivity in such waveguides should be mainly controlled by the conductive layer thickness. Müller cells were found to be wavelength-dependent waveguides [46] that collect the green-red part of the visible spectrum onto the photoreceptor cones, allowing the blue-purple part of the spectrum to leak onto nearby rods. This was observed in an isolated retina and explained by a computational model in the guinea pig and human parafoveal retina. The Müller cell transmission spectrum has a broad transmission band [46] with its half-width corresponding to the 530 – 610 nm (16400 – 19230 cm^{-1}) spectral interval. These results may also be interpreted in terms of the quantum mechanism of light transmission in the retina. Analyzing the Müller cell morphology by transmission electron microscopy, we reported that the IF bundles run through the entire Müller cell [11]. Noting that the transmission spectrum of the optical waveguide depends on the conductive layer thickness, we could assume that the IF bundle includes IFs with different thickness of the conductive layer, thus, the Müller cell transmission spectrum will be obtained by a superposition of the transmission spectra of those different types of IFs. The effective transmission spectrum may be thus simulated by adjusting the contributions of the different types of the IFs. The quantum mechanism expects very high light transmission efficiencies by the IFs, therefore the IF bundle should be organized so as to provide very low energy losses. Thus, the transmission spectrum of the Müller cells will be given by:

$$S(\omega)=\sum g_i S_i(\omega) \quad (11)$$

where g_i is the contribution of the IFs with the transmission spectrum $S_i(\omega)$. Therefore, we can build an arbitrary transmission spectrum by producing the required superposition (11), with $S_i(\omega)$ calculated for the diameter distributed in the 10 – 18 nm range and variable thickness ρ of IF conductive layer, and next adjusting the respective spectral contributions. The respective calculations may be done using the theory developed here and earlier [12,13]. As we already noted, the broad transmission spectrum of the Müller cells measured by Labin et al. [46]may be explained by the transmission spectrum of the IF bundle with constant-diameter filaments, provided their conductive layer is sufficiently thick. However, the resulting efficiency of light transmission will be lower (Figure 6a and 6b), compared to the above example. Indeed, presently we report (Figure 6b) that the transmission spectrum of the IF with the internal radius of the conductive nanolayer of 5 nm and 4 nm thickness correlates quite well with the experimental data [46], although the maximum transmission efficiency is only 0.17.

Thus, to optimize the light transmission efficiency by the IFs, we envision a bundle of IFs with different diameters in the 10 – 18 nm range and small conductive layer thickness, of around 1 - 1.5 nm. Such a mixture of IFs could reproduce the transmission over the entire visible spectrum, as an alternative to the constant-diameter IFs with thick conductive walls, which seems simpler from the evolutionary point of view. Apparently we shall need more experimental results on the diameter distribution of the IFs to be able to choose between these two hypotheses.

Quite a lot of research has been devoted to understanding the high contrast of (daylight) vision in animals with an inverted retina. The issue was first put on the table by Solovei et al. [47], who described the classic model of light transmission thought the retina and formulated the difficulties in explaining the high visual contrast (and resolution) achieved by animals. Franze et al. [5] showed that Müller cells are lightguides, with the incident light focused by the conical lenses of their endfeet [11]. However, the classical mechanism results in light scattering by the cellular organelles, reducing contrast and resolution. Therefore, we believe that the proposed earlier [12] and discussed here quantum mechanism of light transmission by way of excitons operates primarily in daylight, achieving high contrast and resolution (with the scattered light suppressed by pigment cells), whereas the classical mechanism operates in low-light conditions, with the contrast and resolution losses traded in for the ultimate single-photon detection sensitivity. Thus, the high contrast and resolution in daylight are provided by the quantum mechanism, with IFs transmitting energy in the form of excitons.

Perspectives

The presently proposed mechanism of retinal light transmission requires additional experimental testing. Once again, carbon nanotubes could make a good model system for such experiments, as the light transmission spectra should differ significantly between single-wall and multi-wall tubes, depending on the number of walls. The respective model studies as well as studies with MC IFs are planned for the nearest future.

V. Conclusions

We report that model waveguides shown in Figs. 2 and 4 are spectrally selective as regards light transmission. The position and width of the spectral transmission maximum depend on the fiber diameter and conductive layer thickness and shape, making it an efficient nano-sized optical filter. Similar structures exist in different cells, including Müller cells. Namely, a bundle of specialized intermediate filaments goes through the entire Müller cell, conducting light energy from the internal retinal surface to the cone cells in the photoreceptor layer.

Presently we discussed the spectral selectivity of the specialized intermediate filaments in Müller cells. As we already noted, apparently all of the live organisms with an inverted retina have intermediate filaments that transmit light. We infer that these light-transmitting intermediate filaments should be spectrally selective, similarly to those of the presently discussed model systems, provided they have a structure similar to that of a cylinder with conductive surface layer. Taking into account high transparency of the nanostrucured

waveguides in a narrow spectral band, we propose that a bundle containing intermediate filaments with different diameters may efficiently transmit photons in the entire visible spectral range. Since the light transmission efficiency of a single intermediate filament is very high, achieving 0.8 – 0.9, the light transmission by a bundle of intermediate filaments should have the same high efficiency in the broad spectral region; thus, the spectral selectivity of the IFs creates high efficiency of the retinal light transmission. We demonstrated the proposed mechanism experimentally, using a macroscopically-sized model waveguide with one of the dimensions in the nanometer range. Further development of the quantum mechanism [11,12] will provide comprehensive interpretation of the retinal light transmission in the inverted retina, including the energy transfer from the intermediate filament bundle to the photoreceptors. The quantum exciton transport mechanism complements the classical optical light guide mechanism, operating in daylight and providing high contrast and resolution, whereas the classical mechanism operates in night vision, providing the ultimate photon detection sensitivity at a cost of reduced resolution.

Acknowledgments

The authors are grateful for the NASA EPSCoR grant PR NASA EPSCoR (NASA Cooperative Agreement NNX13AB22A) to V. M., NIH grant G12 MD007583 to M. I., and Russian Science Foundation grant 16-14-10159 to L. Z.

References

1. Li T, Zhou X, Luo X, Jiang B. Int J Clin Exp Med. 2016; 9:7080–7087.
2. Buttery RG, Hinrichsen CF, Weller WI, Haight JR. Vision Res. 1991; 31:169–87. [PubMed: 2017880]
3. Chan, Annie, Duker, Jay S., Ko, Tony H., Fujimoto, James G., Schuman, Joel S. Arch Ophthalmol. 2006; 124:193–198. HHS Public Access. DOI: 10.1001/archopht.124.2.193 [PubMed: 16476888]
4. Robert, D., editor. Celular Molecular Biologyof Intermediate Filaments. Goldman Northwestern University Medical School Chicago, Illinois and Peter M. Steinert National Cancer Institute National Institutes of Health Bethesda, Maryland: Springer cience+Business Media, LLC; 1990.
5. Franze K, Grosche J, Skatchkov SN, Schinkinger S, Foja C, Schild D, Uckermann O, Travis K, Reichenbach A, Guck J. PNAS. 2007; 104:8287–8292. DOI: 10.1073/pnas.0611180104 [PubMed: 17485670]
6. Wu PC, Chen YJ, Chen CH, Chen YH, Shin SJ, Yang HJ, Kuo HK. Eye. 2008; 22:551–555. published online 27 April 2007. DOI: 10.1038/sj.eye.6702789 [PubMed: 17464309]
7. Dreher Z, Robinson RS, Distler C. The Journal of Comparative Neurology. 1992; 323:59–80. [PubMed: 1430315]
8. Clark JL, Matsushima H, David LL, Clark JM. Eye (Lond). 1999; 13:417–24. [PubMed: 10627819]
9. Reichenbach A, Bringmann A. Müller Cells in Healthy and Diseased Retina, Springer. 2010
10. Ruggeri M, Major JC Jr, McKeown C, Knighton RW, Puliafito CA, Jiao S. Investigative Ophthalmology & Visual Science. 2010; 51:5789–5795. [PubMed: 20554605]
11. Zueva L, Golubeva T, Korneeva E, Makarov V, Khmelinskii I, Inyushin M. Microsc Microanal. 2016; :1–8. DOI: 10.1017/S1431927616000507
12. Makarov V, Zueva L, Golubeva T, Korneeva E, Khmelinskii I, Inyushin M. J Neurophotonics. 2016; 4:1–14. 011005.
13. Khmelinskii I, Zueva L, Inyushin M, Makarov V. Photonics and Nanostructures – Fundamentals and Applications. 2015; 16:24–33. [PubMed: 26435707]
14. Oka M, Kudo H, Sugama N, Asami Y, Takehana M. Mol Vis. 2008; 25:815–22.

15. Goyal, S., Kim, Y-tae, Iqbal, SM. Effect of Fluorescent Tags on Translocation through Nanochannels; 32nd Annual International Conference of the IEEE EMBS; Buenos Aires, Argentina. August 31 - September 4, 2010;
16. Kohli P, Harrell CC, Cao Z, Gasparac R, Tan W, Martin CR. Science. 2004; 305:984. [PubMed: 15310896]
17. Moreira BG, You Y, Behlke MA, Owczarzy R. Biochemical and Biophysical Research Communications. 2005; 327:473. [PubMed: 15629139]
18. McNamara G, Gupta A, Reynaert J, Coates TD, Boswell C. Spectral imaging microscopy web sites and data, Cytometry Part A. 2006; 69:863.
19. Chen, Li, Zhou, W., Qiang, Z., Brown, GJ. Spectral Selectivity of Photonic Crystal Infrared Photodetectors, Nanomaterial Synthesis and Integration for Sensors, Electronics, Photonics, and Electro-Optics. In: Dhar, NK.Dutta, AK., Islam, MS., editors. Proc of SPIE. Vol. 6370. 2006. p. 63701I-1.
20. Krier A. Mid-infrared semiconductor optoelectronics London: Springer. 2006
21. Lin SY, Fleming JG, Li ZY, El-Kady I, Biswas R, Ho KM. Journal of Optical Society America B. 2003; 20:1538.
22. Xi YG, Wang X, Hu XH, Liu XH, Zi J. Chinese Physics Letters. 2002; 19:1819.
23. David SV, Hayden BY, Gallant JL. Journal of Neurophysiology. 2006; 96:3492.doi: 10.1152/jn.00575.2006 [PubMed: 16987926]
24. Adelson EH, Bergen JR. J Opt Soc Am. 1985; A 2, 284
25. Wang J, Karabinos A, Zimek A, Meyer M, Riemer D, Hudson C, Lemaire P, Weber K. Eur J Cell Biol. 2002; 81:302–311. [PubMed: 12067066]
26. Khmelinskii I, Makarov VI. Photonics and Nanostructures - Fundamentals and Applications. 2016; 19:39–47.
27. Khmelinskii I, Makarov V. Journal of Quantitative Spectroscopy and Radiative Transfer. 2016; 175:68–75.
28. Bredfeldt CF, Ringach DL. J Neurosci. 2002; 22:1976. [PubMed: 11880528]
29. http://lofi.forum.physorg.com/Geometrical-Structure-For-Benzene_18603.html.
30. Nelson, PC. Biological Physics, Energy, Information, Life. Freeman, WH., editor. 2004. p. 600
31. Zayats AV, Smolyaninov II. J Opt A: Pure Appl Opt. 2003; 5:S16–S50. 56959.
32. Oulton RF, Sorger VJ, Zentgraf T, Ma RM, Gladden C, Dai L, Bartal G, Zhang X. Nature. 2009; 461:629. [PubMed: 19718019]
33. Chen J, Perebeinos V, Freitag M, Tsang J, Fu O, Liu J, Avouris P. Science. 2005; 310:1171.doi: 10.1126/science.1119177 [PubMed: 16293757]
34. Ron I, Pecht I, Sheves M, Cahen D. Acc Chem Res. 2010; 43:945.doi: 10.1021/ar900161u [PubMed: 20329769]
35. Strelkov SV, Herrmann H, Aebi U. Bioessays. 2003; 25:243–51. [PubMed: 12596228]
36. Song S, Landsbury A, Dahm R, Liu Y, Zhang Q, Quinlan RA. J Clin Invest. 2009; 119:1837–48. [PubMed: 19587458]
37. Frank S, Poncharal P, Wang ZL, de Heer WA. Science. 1998; 280:1744. [PubMed: 9624050]
38. Sinnott SB, Andreys R. Sciences. 2001; 26:145.doi: 10.1080/20014091104189
39. Kataura H, Kumazawa Y, Maniwa Y, Umezu I, Suzuki S, Ohtsuka Y, Achiba Y. Synthetic Metals. 1999; 103:2555.doi: 10.1016/S0379-6779(98)00278-1
40. Iakoubovskii K, Matsui H, Matsuzaki H, Okamoto H, Miyata Y. Journal of Physical Chemistry B. 2006; 110:17420.doi: 10.1021/jp062653t
41. Iakoubovskii K, Minami N, Kazaoui S, Ueno T, Miyata Y, Yanagi K, Kataura H, Ohshima S, Saito T. Journal of Physical Chemistry C. 2008; 112:11194.doi: 10.1021/jp8018414
42. Joannopoulus, JD., Meade, RD., Winn, JN. Photonic Crystals. Princeton, NJ: Princeton University Press; 1995.
43. Iakoubovskii K, Minami N, Kazaoui S, Ueno T, Miyata Y, Yanagi K, Kataura H, Ohshima S, Saito T. Applied Physics Letters. 2006; 89:173108.doi: 10.1063/1.2364157
44. Mintmire JW, White CT. Phys Rev Lett. 1998; 81:2506.

45. Bedford, NM., Munro, CJ., Knecht, MR. Peptide Bindinf for Bio-Based Nanomaterials, Peptode, Proteine, Enzymes. Picoraro, Vincento L., editor. Vol. 580. 2007. p. 581-633.

46. Amichai, M Labin, Shadi, K Safuri, Erez, N Ribak, Ido, Perlman. Nature Communications. 2014; 5:431:1–9. DOI: 10.1038/ncomms5319

47. Solovei I, Kreysing M, Lancto C, Kosem S, Peichl L, Cremer T, Guck J, Joff B. Cell. 2009; 137:356–368. [PubMed: 19379699]

Highlights

Development of a new theoretical models of light transmission of nano channels;

Development of quantum models of light transmission by intermediate filaments;

Development of theory of experimental methods to prove theoretical models.

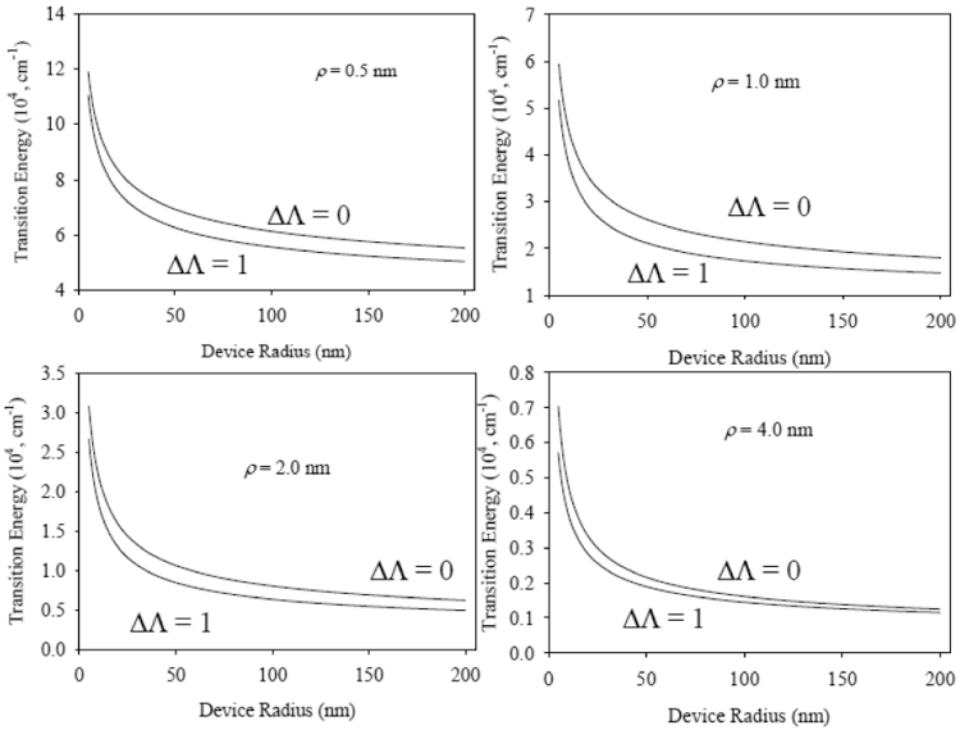

Figure 1.

The internal radius r_0 dependences of the spectral absorption maximum of a cylindrical tube at ρ= 0.5, 1.0, 2.0 and 4.0 nm, and tube length of 100 μm.

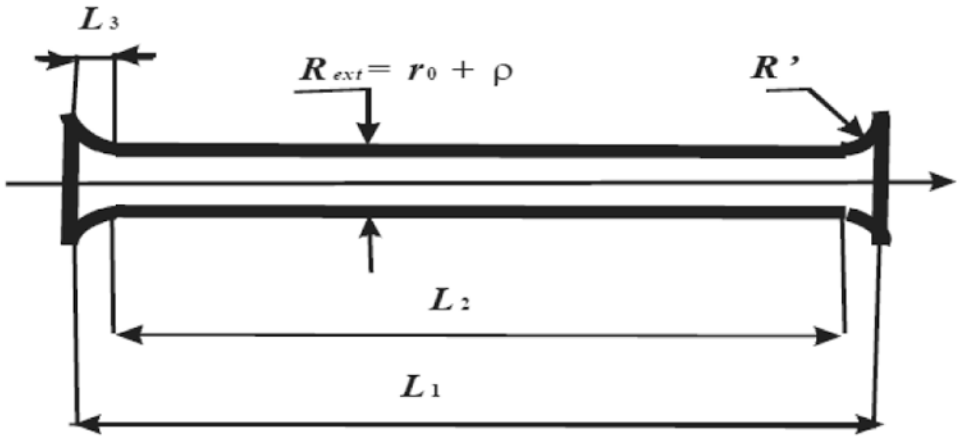

Figure 2.
Geometry of the waveguide used in the numerical analysis.

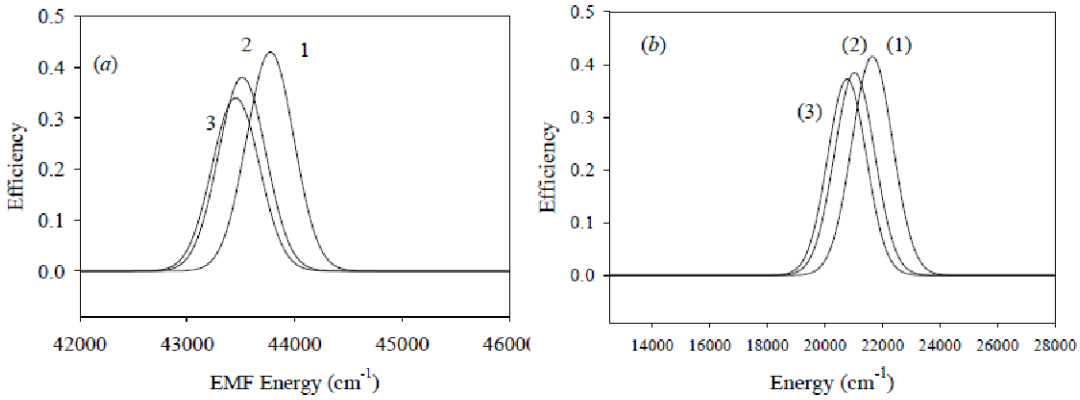

Figure 3.

(1) Absorption efficiency, (2) energy transmission efficiency and (3) EMF emission efficiency spectra of the waveguides: (*a*) ρ= 0.5 nm, r_0 = 5 nm, L_1 = 100 μm, L_2 = 99.990 μm, L_3 =5 *nm* and R = 5.5 nm; (*b*) ρ= 1.0 nm, r_0 = 5 nm, L_1 = 100 μm, L_2 = 99.990 nm, L_3 =5 *nm* and R = 5.5 nm.

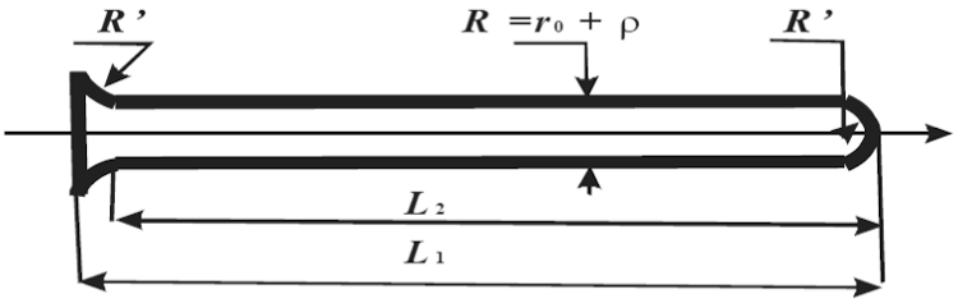

Figure 4.
The waveguide model.

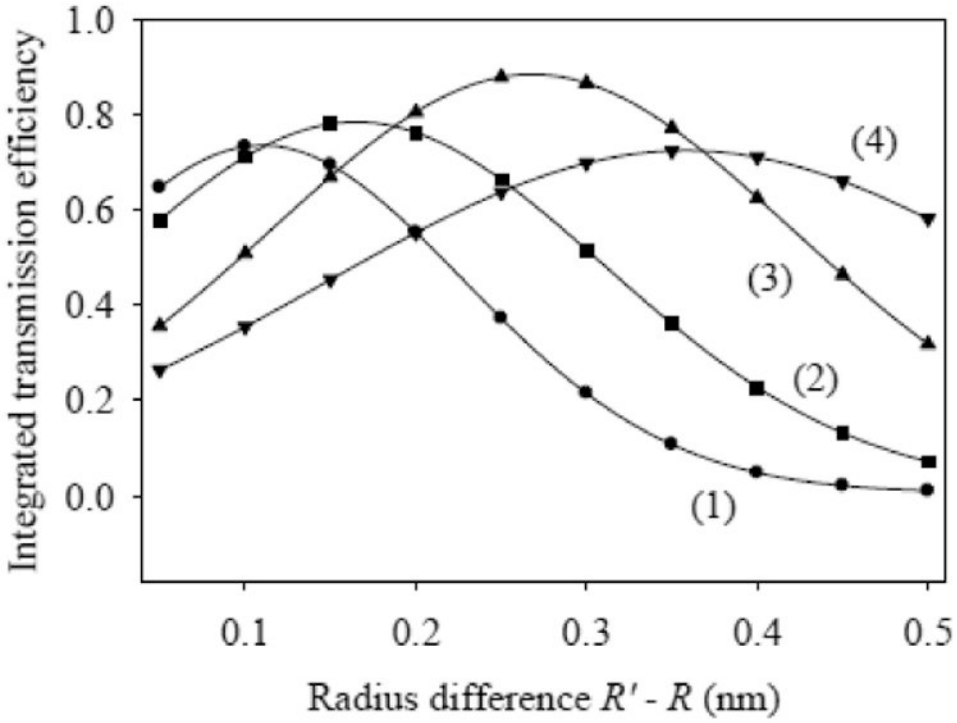

Figure 5.

Numerical analysis of the EMF transmission efficiency for the waveguide of Figure 4 with the following parameter sets: (1) ρ= 0.5 nm, L_1 = 100 μm, L_2 = 99.995 μm, r_0 =2.5 nm, R=3 nm; (2) r_0 =5 nm, R =5.5 nm, other parameters are the same; (3) r_0 = 7.5 nm, R =8 nm, all of the other parameters are the same; (4) r_0 = 10 nm, R =10.5 nm, all of the other parameters are the same.

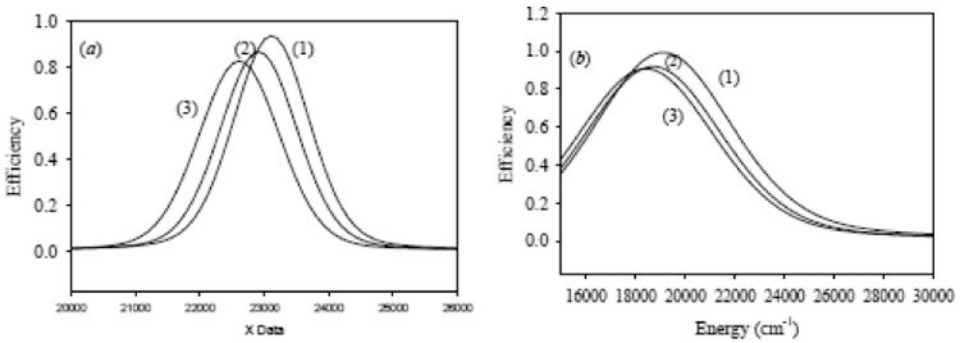

Figure 6.

Calculated for the device of Figure 4: (1) absorption, (2) transmission and (3) emission spectra, respectively. The waveguide parameters are: (a) ρ= 1.0 nm, r_0 = 5 nm, R' = 6 nm, L_1 = 100 μm, L_2 = 99.995 μm and (*b*) ρ= 4.0 nm, r_0 = 5 nm, R' = 9 nm, L_1 = 100 μm, L_2 = 99.995 μm.

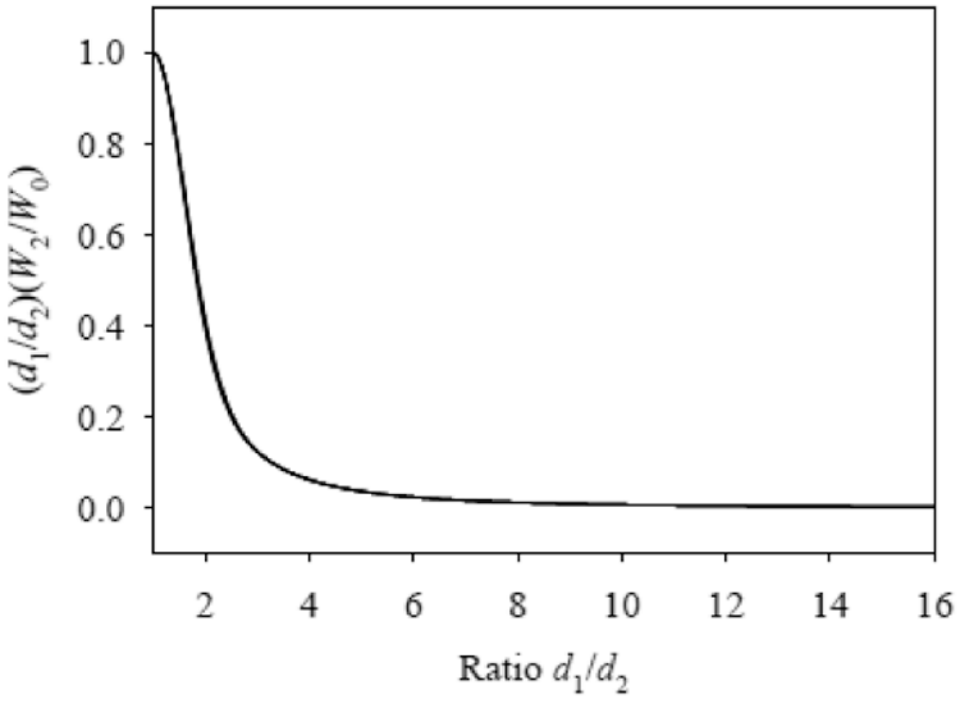

Figure 7.

The EMF power transmitted from one optical fiber to another vs. the d_1/d_2 ratio at different input powers, with all plots coincident; the input power varied from 5 μW to 10 μW.

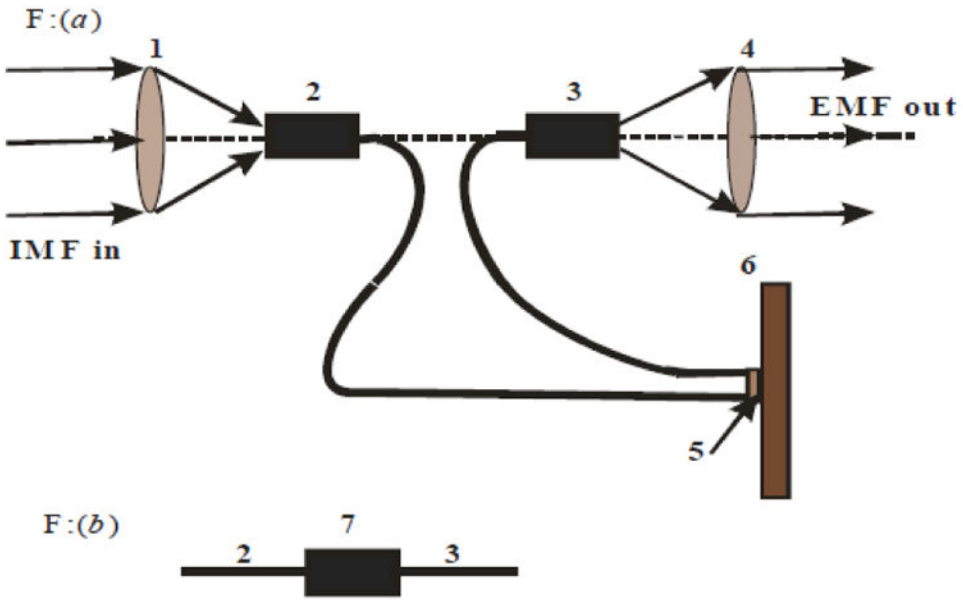

Figure 8.

Schematic presentation of the assembly used to record the transmission spectra of Cr nanotracks deposited on AlN substrate: (*a*) transmission measurements (1) – focusing lens for the probing light; (2), (3) – fiber optic cable; (4) – defocusing lens for the probing light; (5) – Cr nanotrack; (6) – AlN substrate; (*b*) background measurement: (2), (3) – the two fiber optic cables; (7) – fiber optic connector.

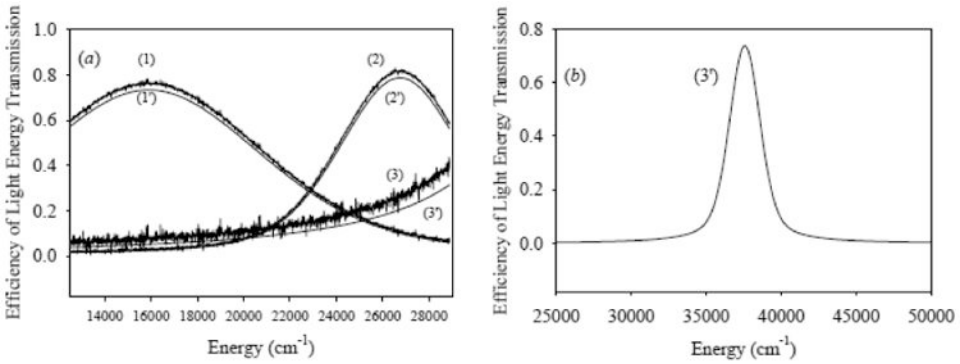

Figure 9.

Experimental and theoretical spectra of Cr nanotracks: (*a*) (1) – experimental spectrum for 8.3 nm Cr nanotrack, (1′) – calculated spectrum for 8.3 nm Cr nanotrack; (2) – experimental spectrum for 6.4 nm Cr nanotrack, (2′) – calculated spectrum for 6.4 nm Cr nanotrack; (3) – experimental spectrum for 5.1 nm Cr nanotrack, (3′) – calculated spectrum for 5.1 nm Cr nanotrack; (b) (3′) calculated spectrum for a Cr nanotrack 5.1 nm thick.

Table 1

The values of the ω_0 and σ fitting parameters for the two different parameter sets.

(*a*) ρ= 0.5 nm; r_0 = 5 nm; L_1 = 100 μm; L_2 = 99.99 μm; L_3 = 5 nm; R = 5.5 nm.		
Band Number	**ω_0, cm^{-1}**	**σ, cm^{-1}**
(1)	43773	220
(2)	43514	221
(3)	43453	223
(*b*) ρ = 1.0 nm; r_0 = 5 nm; L_1 = 100 μm; L_2 = 99.99 μm; L_3 = 5 nm; R = 5.5 nm.		
Band Number	ω_0, cm^{-1}	σ, cm^{-1}
(1)	21646	709
(2)	21030	696
(3)	20766	672

Table 2

The values of the fitting parameters of ω_0 and σ for the two different parameter sets.

(*a*) ρ= 1.0 nm, r_0 = 5 nm, R' = R = 6 nm, L_1 = 100 μm, L_2 = 99.995 μm.		
Band Number	**ω_0, cm^{-1}**	**σ, cm^{-1}**
(1)	23110	602
(2)	22910	613
(3)	640	22610
(*b*) ρ= 4.0 nm, r_0 = 5 nm, R' = R = 9 nm, L_1 = 100 μm, L_2 = 99.995 μm.		
Band Number	ω_0, cm^{-1}	σ, cm^{-1}
(1)	19119	2754
(2)	18719	2748
(3)	18419	2750